Finite Extension of Accreting Nonlinear Elastic Solid Circular Cylinders*

Arash Yavari[†1,2], Yasser Safa[3], and Arash Soleiman Fallah[4]

[1] *School of Civil and Environmental Engineering, Georgia Institute of Technology, Atlanta, GA 30332, USA*
[2] *The George W. Woodruff School of Mechanical Engineering, Georgia Institute of Technology, Atlanta, GA 30332, USA*
[3] *Institute for Computational Physics, School of Engineering, ZHAW - Zurich University of Applied Sciences, 8400 Winterthur, Switzerland*
[4] *Department of Mechanical, Electrical and Chemical Engineering, Oslo Metropolitan University, 0166 Oslo, Norway*

March 1, 2023

Abstract

In this paper we formulate and solve the initial-boundary value problem of accreting circular cylindrical bars under finite extension. We assume that the bar grows by printing stress-free cylindrical layers on its boundary cylinder while it is undergoing a time-dependent finite extension. Accretion induces eigenstrains, and consequently residual stresses. We formulate the anelasticity problem by first constructing the natural Riemannian metric of the growing bar. This metric explicitly depends on the history of deformation during the accretion process. For a displacement-control loading during the accretion process we find the exact distribution of stresses. For a force-control loading, a nonlinear integral equation governs the kinematics. After unloading there are, in general, a residual stretch and residual stresses. For different examples of loadings we numerically find the axial stretch during loading, the residual stretch, and the residual stresses. We also calculate the stress distribution, residual stretch, and residual stresses in the setting of linear accretion mechanics. The linear and nonlinear solutions are numerically compared in a few accretion examples.

Keywords: Accretion mechanics, surface growth, nonlinear elasticity, residual stress, universal deformations, geometric mechanics.

1 Introduction

There are many examples of accretion (surface or boundary growth) in nature, e.g., the growth of biological tissues and crystals, the build-up of volcanic and sedimentary rocks, of ice structures, the formation of planets, etc., and in engineering applications, e.g., additive manufacturing (3D printing), metal solidification, the build-up of concrete structures in successive layers, the deposition of thin films, and ice accretion on an aircraft wing that leads to degradation of aerodynamic performance, etc. Accretion can be visualized in terms of the formation of non-Euclidean solids—a term that was coined by Poincaré [1905]—through a continuous joining of infinitely many two-dimensional layers [Zurlo and Truskinovsky, 2017, 2018]. This is mathematically described by a foliation of the material manifold [Sozio and Yavari, 2019]. The first theoretical study of accretion mechanics is due to Southwell [1941]. One of the first problems that was solved in the setting of linear accretion mechanics is the problem of a growing planet subject to self-gravity [Brown and Goodman, 1963]. Metlov [1985] proposed the first finite deformation theory of accretion and

*To appear in *Continuum Mechanics and Thermodynamics*.
†Corresponding author, e-mail: arash.yavari@ce.gatech.edu

introduced a time of attachment map. There are many more works in the literature of the mechanics of accretion [Drozdov, 1998a,b, Arutyunyan et al., 1990, Manzhirov, 1995, Ong and O'Reilly, 2004, Kadish et al., 2005, Epstein, 2010, Lychev and Manzhirov, 2013, Manzhirov, 2014, Lychev, 2017, Lychev et al., 2021, Tomassetti et al., 2016, Sozio and Yavari, 2017, 2019, Sozio et al., 2020, Abi-Akl et al., 2019, Abi-Akl and Cohen, 2020, Truskinovsky and Zurlo, 2019, Bergel and Papadopoulos, 2021]. For a detailed literature review of the mechanics of accretion see [Naumov, 1994, Sozio and Yavari, 2017].

In nonlinear accretion mechanics one is interested in the state of deformation and stress of a body undergoing large deformations while new material is being added on part of its boundary. Accretion is a source of anelasticity (in the sense of Eckart [1948]), and hence, residual stresses. There are recent geometric formulations that model the accretion-induced anelasticity by a Riemannian material manifold whose metric explicitly depends on the history of deformation during accretion [Sozio and Yavari, 2017, 2019, Sozio et al., 2020, Yavari and Pradhan, 2022]. In this paper we consider symmetric accretion of a finite solid circular cylinder made of an arbitrary incompressible isotropic solid. We construct the material manifold of an accreting bar that is under a time-dependent finite extension and calculate its stresses and deformation during accretion. We consider both displacement and force-control loadings during accretion. Next, the residual stretch and residual stresses are calculated. Finally, the same analysis is repeated in the setting of linearized accretion mechanics.

The examples discussed in this paper are motivated by problems encountered in additive manufacturing of cylindrical-shaped samples under axial loads during accretion. The methods introduced in the present paper for accretion analysis provide theoretical insights for additive manufacturing applications. More specifically, in additive manufacturing controlling the residual stress field induced during layers deposition is crucial. It should be noted that residual stresses can potentially affect the service integrity of additively-manufactured products in different ways. For instance, residual tensile stresses can cause the corrosion onset and subsequent stress-corrosive crack propagation in additively-manufactured metallic parts [Nazarov et al., 2019]. Tensile residual stresses can also increase the pores size in 3D-printed samples [Colegrove et al., 2017] and have a detrimental effect on their fatigue life [Kalentics et al., 2017]. Several techniques have been proposed to manage the residual stress development, prevention, and compensation in additive manufacturing [Carpenter and Tabei, 2020]. Some of such techniques are based on applying external mechanical forces during accretion. Such forces can be locally applied e.g., the waves generated by laser shock peening to improve the product quality of selective laser melting [Kalentics et al., 2017]. External forces can also be globally applied during layer deposition, e.g., the bulk deformation using punch rolling techniques [Colegrove et al., 2017, Tangestani et al., 2020]. Application of such global forces can provide significant benefits including reducing residual stresses and distortion, and improving the quality of the additively-manufactured parts. The effect of bulk deformation on the mitigation of distortion due to material shrinkage and residual stresses induced during an additive manufacturing process has been a subject of research in recent years. As an example, a computational model involving a pre-distortion of the design geometry based on 3D optical scanning measurement data was implemented with reported benefits on achievable compensation of residual stresses in [Afazov et al., 2017]. To our knowledge, in the literature there are no models that can predict the effects of time-dependent bulk deformation treatments during accretion. Similar to pre-stretching treatments to reduce the residual stresses deriving from quenching processes [Zhu and Yuan, 2021], application of external forces during an additive manufacturing process affects the distribution of residual stresses. A quantitative understanding of such effects is crucial in the design of additively manufactured structures.

This paper is organized as follows. In §2, we formulate and solve the initial-boundary-value problem of accretion of a circular cylindrical bar under a time-dependent finite extension. We show that kinematics is fully determined by the axial stretch function. We consider both displacement-control and force-control loadings. Calculation of residual stresses is discussed in §2.1. The accretion analysis in the setting of linearized accretion mechanics is presented in §2.2. For a few examples of force-control loadings during accretion we compare the axial stretch calculated using the linear and nonlinear theories. Conclusions are given in §3.

2 Finite extension of an accreting circular cylindrical bar

In this section we formulate and solve the initial-boundary value problem of symmetric accretion of a circular cylindrical bar made of an incompressible[1] isotropic hyperelastic solid that is undergoing a time-dependent finite extension while stress-free cylindrical layers are added to its boundary cylinder (see Fig.1).

Kinematics and the material metric. Let us consider a circular cylindrical bar with initial length L and radius R_0 that is made of a homogeneous isotropic and incompressible material ($I_3 = 1$) with an energy function $W = W(I_1, I_2)$, where I_1, I_2, I_3 are the principal invariants of the right (or left) Cauchy-Green tensors [Ogden, 1997]. We use the cylindrical coordinates (R, Θ, Z) and (r, θ, z) in the reference and current configurations, respectively. The metrics of the reference and current configurations of the initial body ($0 \le R \le R_0$) have the following representations

$$\mathbf{G} = \begin{bmatrix} 1 & 0 & 0 \\ 0 & R^2 & 0 \\ 0 & 0 & 1 \end{bmatrix}, \quad \mathbf{g} = \begin{bmatrix} 1 & 0 & 0 \\ 0 & r^2 & 0 \\ 0 & 0 & 1 \end{bmatrix}. \tag{2.1}$$

Let us consider a time-dependent extension of the circular cylindrical bar such that it is slow enough for the inertial effects to be negligible. Finite extensions of a circular cylindrical bar are represented by the following family of maps:[2]

$$r = r(R,t)\,, \quad \theta = \Theta\,, \quad z = \lambda^2(t) Z\,, \qquad t \in [0, t_a]\,, \tag{2.2}$$

where $\lambda^2(t)$ is the axial stretch.[3] We can assume that this is a displacement-control loading for which $\lambda(t)$ is given. Alternatively, one can assume that the applied axial force is given and in that case $\lambda(t)$ is an unknown function to be determined. The deformation gradient reads

$$\mathbf{F} = \mathbf{F}(R,t) = \begin{bmatrix} r'(R,t) & 0 & 0 \\ 0 & 1 & 0 \\ 0 & 0 & \lambda^2(t) \end{bmatrix}, \tag{2.3}$$

where $r'(R,t) = \frac{\partial r(R,t)}{\partial R}$. The deformation tensors $\mathbf{c}^\flat$ and $\mathbf{b}^\sharp$ (the Finger deformation tensor) are defined as

$$\begin{aligned} \mathbf{c}^\flat &= \varphi_* \mathbf{G}\,, \qquad c_{ab} = \big(F^{-1}\big)^A{}_a \big(F^{-1}\big)^B{}_b \, G_{AB}\,, \\ \mathbf{b}^\sharp &= \varphi_* \mathbf{G}^\sharp\,, \qquad b^{ab} = F^a{}_A \, F^b{}_B \, G^{AB}. \end{aligned} \tag{2.4}$$

Notice that $b^{ac}\, c_{cb} = b^a{}_m \, c^m{}_b = \delta^a_b$, i.e., $\mathbf{b} = \mathbf{c}^{-1}$.

The incompressibility condition is written as

$$J = \sqrt{\frac{\det \mathbf{g}}{\det \mathbf{G}}}\, \det \mathbf{F} = \frac{r(R,t)}{R}\, r'(R,t)\, \lambda^2(t) = 1\,. \tag{2.5}$$

This condition, together with $r(0,t) = 0$, gives us

$$r(R,t) = \frac{R}{\lambda(t)}\,, \qquad 0 \le R \le R_0\,. \tag{2.6}$$

We assume that while the cylindrical bar is under the time-dependent deformation (2.2) cylindrical layers of stress-free material are printed continuously on its boundary (see Fig.1). The growth velocity is assumed

[1] The accretion formulation presented in this paper is not restricted to incompressible solids. However, incompressibility simplifies the kinematics.

[2] The set of finite extensions of circular cylindrical bars is a subset of Family 3 deformations that are universal for incompressible isotropic solids [Ericksen, 1954]. They are universal for certain inhomogeneous and anisotropic bars as well [Yavari, 2021a, Yavari and Goriely, 2021, 2022]. In this paper, we restrict our calculations to isotropic and homogeneous bars. However, our analysis can be extended to certain inhomogeneous and anisotropic bars.

[3] We assume that maximum of $\lambda(t)$ for $t \in [0, t_a]$ is small enough such that radial deformations are the only possible deformations, i.e., we are not considering instabilities either during loading or unloading.

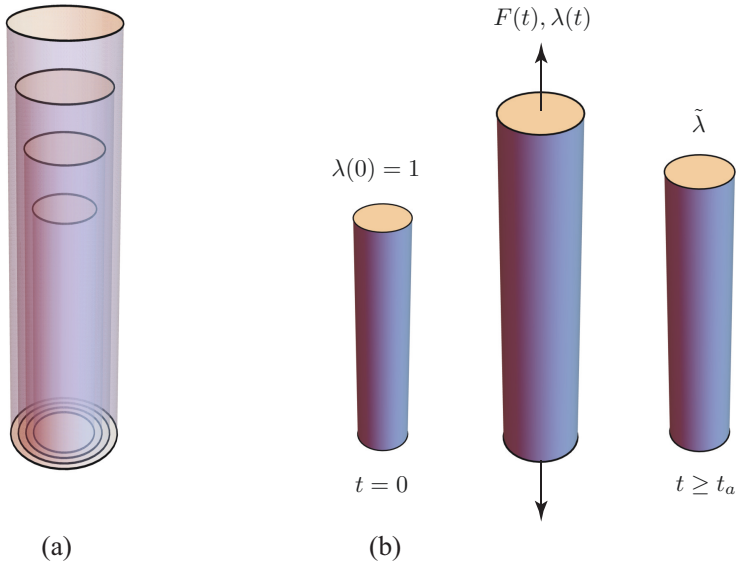

Figure 1: *(a) An accreting circular cylindrical bar undergoing finite extensions. (b) The initial bar, the accreting bar at time t, and the residually-stressed accreted bar after the completion of accretion and removal of the external forces.*

to be normal to the boundary in the current configuration and has magnitude $u_g(t)$. This means that in the time interval $[t, t+dt]$ a stress-free circular cylindrical shell of thickness $u_g(t)\,dt$ is attached to the deformed body (see Fig.2). We also assume that this accretion process is continuous in the time interval $t \in [0, t_a]$. Let us assign a time of attachment $\tau(R)$ to the layer with the radial coordinate R in the reference configuration. For $0 \leq R \leq R_0$, $\tau(R) = 0$. We assume that there is no ablation during the accretion process, and hence $\tau(R)$ is invertible for $R > R_0$. Its inverse is denoted by $s = \tau^{-1}$ and assigns to the time t the radial coordinate of the accreted cylinder in the reference configurations. The growth surfaces in the reference and the current configuration are defined as

$$\begin{aligned} \Omega_t &= \{(s(t), \Theta, Z) : 0 \leq \Theta < 2\pi\,, 0 \leq Z \leq L\}\,, \\ \omega_t &= \left\{(r(s(t), t), \Theta + \tau(t)Z, \lambda^2(t)Z) : 0 \leq \Theta < 2\pi\,, 0 \leq Z \leq L\right\}\,. \end{aligned} \tag{2.7}$$

Note that

$$\frac{d}{dt} r(s(t), t) = \frac{\partial r}{\partial R}(s(t), t)\dot{s}(t) + \frac{\partial r}{\partial t}(s(t), t) = r'(s(t), t)\; U_g(t) + V^r(s(t), t), \tag{2.8}$$

where $U_g(t) = \dot{s}(t)$, and $V^r = \frac{\partial r}{\partial t}$ is the radial component of the material velocity on the growth surface. In the absence of accretion, the spatial velocity of the material points lying on the boundary is $V^r(s(t), t)$, and this implies that

$$u_g(t) = r'(s(t), t)\, U_g(t)\,. \tag{2.9}$$

Following [Sozio and Yavari, 2017], we choose $U_g(t) = u_g(t)$. Sozio and Yavari [2017] showed that other choices for $U_g(t)$ result in isometric material metrics (see also Yavari and Pradhan [2022]). In other words, this choice will not affect the calculation of deformation and stresses. From (2.9), the choice $U_g(t) = u_g(t)$ imposes the following constraint on $r(R, t)$:

$$r'(s(t), t) = 1\,, \text{ or } \qquad r'(R, \tau(R)) = 1\,. \tag{2.10}$$

We also have $s(t) = R_0 + \int_0^t u_g(\xi) d\xi$. In order to simplify the calculations, let us assume that the spatial growth velocity is constant, i.e., $u_g(t) = u_0 > 0$. However, our formulation is not restricted to this choice. Thus

$$s(t) = R_0 + u_0 t\,, \text{ or } \qquad \tau(R) = \frac{R - R_0}{u_0}\,. \tag{2.11}$$

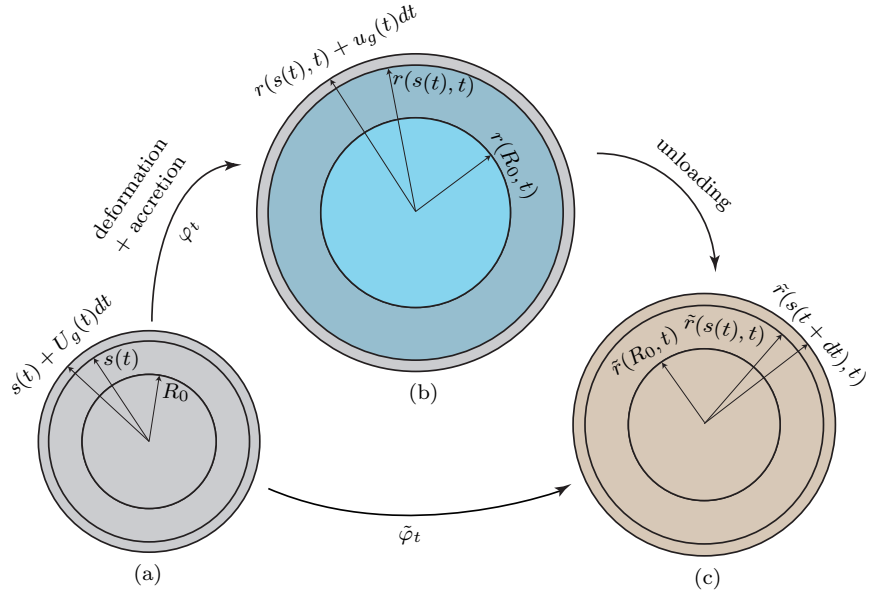

Figure 2: *Cross section of a circular cylindrical bar undergoing symmetric accretion and finite extension simultaneously. (a) The material manifold* $(\mathcal{B},\mathbf{G})$. *The radial coordinate of the accreting bar at time* t *is* $s(t)$. *At a later time* $t+dt$ *the radial coordinate changes to* $s(t)+U_g(t)\,dt$. *(b) The deformed bar under finite extension with a layer of stress-feee material of thickness* $u_g(t)\,dt$ *joining its boundary during the time interval* $[t,t+dt]$. *(c) The residually-stressed accreted bar after the removal of external forces.*

The constraint (2.10) is simplified to read

$$r'(R_0+u_0t,t)=1\,,\ \text{or}\qquad r'\Big(R,\frac{R-R_0}{u_0}\Big)=1\,. \tag{2.12}$$

For the initial body $(0\le R\le R_0)$, the material metric has the representation $(2.1)_1$. For the secondary body $(R_0\le R\le s(t))$, we assume that the accreted cylindrical layer at any instant of time t is stress-free. This implies that the material metric at $R=s(t)$ is the pull-back of the metric of the (Euclidean) ambient space, i.e.,

$$\mathbf{G}(s(t))=\varphi_t^*\mathbf{g}(r(s(t),t))\,,\ \text{or}\qquad \mathbf{G}(R)=\varphi_{\tau(R)}^*\,\mathbf{g}(r(R,\tau(R)))\,. \tag{2.13}$$

In components, $G_{AB}(s(t))=G_{AB}(R)=F^a{}_A(R,\tau(R))\,F^b{}_B(R,\tau(R))\,g_{ab}(r(R,\tau(R)))$. Therefore

$$\mathbf{G}(R)=\begin{bmatrix}r'^2(R,\tau(R)) & 0 & 0\\ 0 & r^2(R,\tau(R)) & 0\\ 0 & 0 & \lambda^4(\tau(R))\end{bmatrix}=\begin{bmatrix}1 & 0 & 0\\ 0 & r^2(R,\tau(R)) & 0\\ 0 & 0 & \lambda^4(\tau(R))\end{bmatrix}, \tag{2.14}$$

where use was made of (2.10), and $\tau(R)$ is given in $(2.11)_2$.

For this accretion problem, the material manifold is an evolving Riemannian manifold $(\mathcal{B}_t,\mathbf{G})$, where

$$\mathcal{B}_t=\{(R,\Theta,Z):0\le\Theta<2\pi\,,\ R_0\le R\le s(t)=R_0+u_0t\,,\ 0\le Z\le L\}\,, \tag{2.15}$$

and

$$\begin{aligned}0\le R\le R_0:\ \ \mathbf{G}&=\begin{bmatrix}1 & 0 & 0\\ 0 & R^2 & 0\\ 0 & 0 & 1\end{bmatrix},\\ R_0\le R\le R_0+u_0t:\ \ \mathbf{G}&=\begin{bmatrix}1 & 0 & 0\\ 0 & \bar{r}^2(R) & 0\\ 0 & 0 & \lambda^4(\tau(R))\end{bmatrix},\quad \bar{r}(R):=r(R,\tau(R))=r\left(R,\frac{R-R_0}{u_0}\right).\end{aligned} \tag{2.16}$$

Remark 2.1. The Riemman curvature tensor in a local coordinate chart $\{X^A\}$ for the material manifold $(\mathcal{B}, \mathbf{G})$ has the following components

$$R^A{}_{BCD} = \frac{\partial \Gamma^A{}_{BD}}{\partial X^C} - \frac{\partial \Gamma^A{}_{BC}}{\partial X^D} + \Gamma^A{}_{CE}\Gamma^E{}_{BD} - \Gamma^A{}_{DE}\Gamma^E{}_{BC}\,, \tag{2.17}$$

where the Christoffel symbols are defined as

$$\Gamma^A{}_{BC} = \frac{1}{2}G^{AK}\left(G_{KB,C} + G_{KC,B} - G_{BC,K}\right)\,. \tag{2.18}$$

The Ricci curvature $\boldsymbol{\mathcal{R}}$ is a symmetric second-order tensor that is defined as $\mathcal{R}_{CD} = R^A{}_{CAD}$. In dimension three, the Ricci curvature completely determines the Riemann curvature of the metric. For $0 \le R \le R_0$, $\boldsymbol{\mathcal{R}} = \mathbf{0}$, while for $R_0 \le R \le R_0 + u_0 t$ it is diagonal with the following components:[4]

$$\begin{aligned}
\mathcal{R}_{RR}(R,t) &= -\frac{\bar{r}''(R)}{\bar{r}(R)} - 2\,\frac{\lambda(\tau(R))\,\lambda''(\tau(R)) + \lambda'^2(\tau(R))}{u_0^2\,\lambda^2(\tau(R))}\,,\\
\mathcal{R}_{\Theta\Theta}(R,t) &= \bar{r}(R)\left[-\bar{r}''(R) - 2\,\frac{\bar{r}'(R)\,\lambda'(\tau(R))}{u_0\,\lambda(\tau(R))}\right]\,,\\
\mathcal{R}_{ZZ}(R,t) &= -2\lambda^2(\tau(R))\;\frac{\lambda(\tau(R))\,[u_0\,\bar{r}'(R)\,\lambda'(\tau(R)) + \bar{r}(R)\,\lambda''(\tau(R))] + \bar{r}(R)\,\lambda'^2(\tau(R))}{u_0^2\,\bar{r}(R)}\,.
\end{aligned} \tag{2.19}$$

Notice that Ricci curvature does not vanish, in general. This implies that the material metric is, in general, non-flat, and hence, the presence of residual stresses. In other words, we expect the accreted bar to be residually stressed after the completion of the accretion process and removal of the applied forces.

The incompressibility constraint for $R \ge R_0$ is written as

$$J = \sqrt{\frac{\det \mathbf{g}}{\det \mathbf{G}}}\,\det \mathbf{F} = \frac{r(R,t)}{r(R,\tau(R))\,\lambda^2(\tau(R))}\,r'(R,t)\,\lambda^2(t) = 1\,. \tag{2.20}$$

Thus

$$r(R,t)\,r'(R,t) = \bar{r}(R)\,\frac{\lambda^2(\tau(R))}{\lambda^2(t)}\,. \tag{2.21}$$

Hence

$$r^2(R,t) = \frac{R_0^2}{\lambda^2(t)} + \frac{2}{\lambda^2(t)}\int_{R_0}^{R}\bar{r}(\xi)\,\lambda^2(\tau(\xi))\,d\xi, \quad R_0 \le R \le R_0 + u_0 t\,, \tag{2.22}$$

where use was made of (2.6). Thus

$$\lambda^2(t)\,r^2(R,t) = R_0^2 + 2\int_{R_0}^{R}\bar{r}(\xi)\,\lambda^2(\tau(\xi))\,d\xi\,. \tag{2.23}$$

The right-hand side is time independent, and hence, $\lambda^2(t)\,r^2(R,t)$ is independent of time. In particular, $\lambda^2(t)\,r^2(R,t) = \lambda^2(\tau(R))\,r^2(R,\tau(R))$, and therefore

$$r(R,t) = \frac{\lambda(\tau(R))}{\lambda(t)}\,\bar{r}(R)\,. \tag{2.24}$$

The constraint (2.10) gives the following ordinary differential equation (ODE) for the unknown function $\bar{r}(R)$:

$$\bar{r}'(R) + \frac{\lambda'(\tau(R)\,\tau'(R))}{\lambda(\tau(R))}\,\bar{r}(R) = 1\,, \tag{2.25}$$

[4]All the symbolic computations in this paper were performed using Mathematica Version 12.3.0.0, Wolfram Research, Champaign, IL.

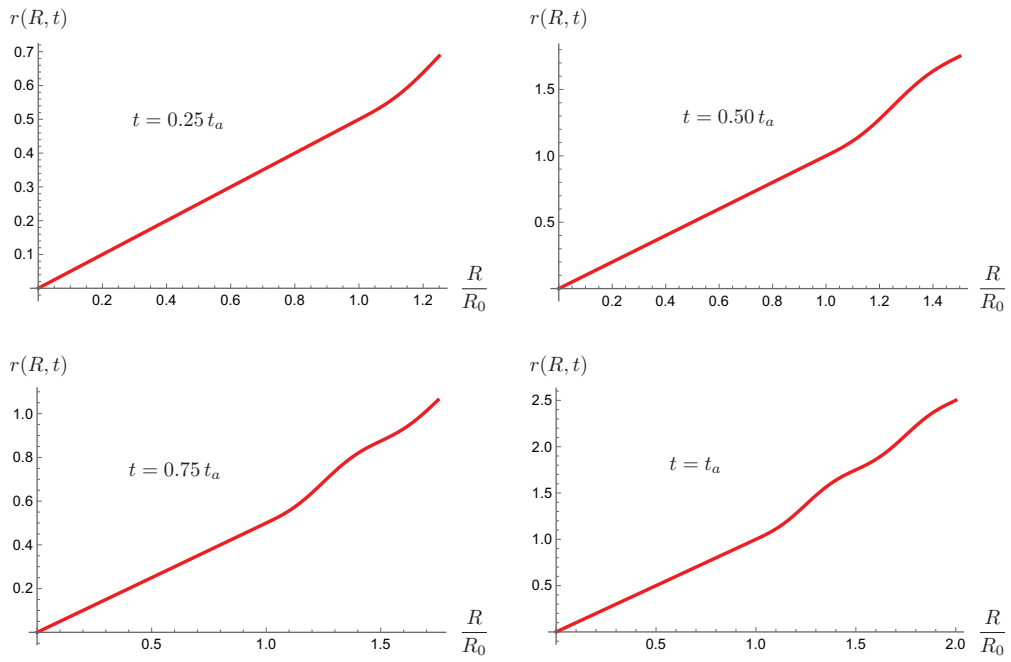

Figure 3: *Radial deformation distribution during the accretion process at four different instances of time for the displacement-control loading* $\lambda(t) = 1 + \sin^2\left(\frac{2\pi\, t}{t_a}\right)$.

which has the following solution:

$$\bar{r}(R) = \frac{1}{\lambda(\tau(R))}\left[R_0 + \int_{R_0}^{R} \lambda(\tau(\xi))\, d\xi\right]. \tag{2.26}$$

Therefore

$$r(R,t) = \frac{1}{\lambda(t)}\left[R_0 + \int_{R_0}^{R} \lambda(\tau(\xi))\, d\xi\right]. \tag{2.27}$$

It is observed that the function $\lambda(t)$ completely determines the kinematics.

Example 2.2. Let us consider the special case of $\lambda(t) = 1$, i.e., accretion with no extension. From (2.6), for $0 \le R \le R_0$, $r(R,t) = R$. For $R \ge R_0$, from (2.27) we have $r(R,t) = R_0 + \int_{R_0}^{R} d\xi = R$. In particular, $\bar{r}(R) = r(R, \tau(R)) = R$. Therefore, from (2.16) for $0 \le R \le R_0 + u_0 t$

$$\mathbf{G} = \begin{bmatrix} 1 & 0 & 0 \\ 0 & R^2 & 0 \\ 0 & 0 & 1 \end{bmatrix}, \tag{2.28}$$

i.e., the material metric is Euclidean, and hence, as expected accretion in the absence of external stretch induces no residual stresses.

Example 2.3. Let us assume that $R_a = 2R_0$, $u_0 = 1$, and $t_a = 1$, and consider a displacement-control loading $\lambda(t) = 1 + \sin^2\left(\frac{2\pi\, t}{t_a}\right)$. In Fig.3 the distributions of radial deformation $r(R,t)$ for four instances of time are shown.

Stresses and equilibrium equations. Next we calculate the stresses in the accreting bar. The principal invariants are defined as $I_1 = \operatorname{tr}\mathbf{b} = b^a{}_a = b^{ab}\, g_{ab}$, $I_2 = \frac{1}{2}\left(I_1^2 - \operatorname{tr}\mathbf{b}^2\right)$ $\frac{1}{2}\left(I_1^2 - b^a{}_b\, b^b{}_a\right) = \frac{1}{2}\left(I_1^2 - b^{ab} b^{cd}\, g_{ac}\, g_{bd}\right)$,

and $I_3 = \det \mathbf{b}$ [Ogden, 1997]. For $0 \le R \le R_0$:

$$\mathbf{b}^\sharp(R,t) = \begin{bmatrix} \frac{1}{\lambda^2(t)} & 0 & 0 \\ 0 & \frac{1}{R^2} & 0 \\ 0 & 0 & \lambda^4(t) \end{bmatrix}, \quad \mathbf{c}^\sharp(R,t) = \begin{bmatrix} \lambda^2(t) & 0 & 0 \\ 0 & \frac{\lambda^4(t)}{R^2} & 0 \\ 0 & 0 & \frac{1}{\lambda^4(t)} \end{bmatrix}. \tag{2.29}$$

The principal invariants of $\mathbf{b}$ read

$$I_1(R,t) = \frac{2+\lambda^6(t)}{\lambda^2(t)}, \quad I_2(R,t) = \frac{1+2\lambda^6(t)}{\lambda^4(t)}. \tag{2.30}$$

Recall that the Cauchy stress for an incompressible isotropic solid has the following representation [Doyle and Ericksen, 1956, Simo and Marsden, 1984]

$$\boldsymbol{\sigma} = -p\,\mathbf{g}^\sharp + 2W_1\,\mathbf{b}^\sharp - 2W_2\,\mathbf{c}^\sharp, \qquad \sigma^{ab} = -p\,g^{ab} + 2W_1\,b^{ab} - 2W_2\,c^{ab}, \tag{2.31}$$

where p is the Lagrange multiplier associated with the incompressibility constraint $J = \sqrt{I_3} = 1$, and $W_i = \frac{\partial W}{\partial I_i}$, $i = 1, 2$. The deformation tensors $\mathbf{c}^\flat$ and $\mathbf{b}^\sharp$ are given in (2.4). Thus, the nonzero components of the Cauchy stress are

$$\begin{aligned} \sigma^{rr}(R,\Theta,Z,t) &= -p(R,\Theta,Z,t) + \frac{\alpha(R,t)}{\lambda^2(t)} - \beta(R,t)\,\lambda^2(t), \\ \sigma^{\theta\theta}(R,\Theta,Z,t) &= -\frac{p(R,\Theta,Z,t)\,\lambda^2(t)}{R^2} + \frac{\alpha(R,t)}{R^2} - \frac{\beta(R,t)\,\lambda^4(t)}{R^2}, \\ \sigma^{zz}(R,\Theta,Z,t) &= -p(R,\Theta,Z,t) + \alpha(R,t)\,\lambda^4(t) - \frac{\beta(R,t)}{\lambda^4(t)}, \end{aligned} \tag{2.32}$$

where $\alpha = 2W_1$ and $\beta = 2W_2$. Using the circumferential and axial equilibrium equations one concludes that $p = p(R,t)$. The radial equilibrium equation reads

$$\frac{\partial \sigma^{rr}}{\partial r} + \frac{1}{r}\sigma^{rr} - r\sigma^{\theta\theta} = 0. \tag{2.33}$$

This can be rewritten in terms of the referential coordinates as $\frac{\partial \sigma^{rr}}{\partial R} = 0$. Thus, $\sigma^{rr}(R,t) = \sigma_0(t)$. This implies that for the initial body one has

$$-p(R,t) = \sigma_0(t) - \frac{\alpha(R,t)}{\lambda^4(t)} + \beta(R,t)\,\lambda^4(t). \tag{2.34}$$

For $R_0 \le R \le R_0 + u_0 t$:

$$\mathbf{b}^\sharp(R,t) = \begin{bmatrix} \frac{\lambda^2(\tau)}{\lambda^2(t)} & 0 & 0 \\ 0 & \frac{1}{\bar{r}^2(R)} & 0 \\ 0 & 0 & \frac{\lambda^4(t)}{\lambda^4(\tau)} \end{bmatrix}, \quad \mathbf{c}^\sharp(R,t) = \begin{bmatrix} \frac{\lambda^2(t)}{\lambda^2(\tau)} & 0 & 0 \\ 0 & \frac{1}{r^2(R,\tau)}\frac{\lambda^4(t)}{\lambda^4(\tau)} & 0 \\ 0 & 0 & \frac{\lambda^4(\tau)}{\lambda^4(t)} \end{bmatrix}. \tag{2.35}$$

The principal invariants of $\mathbf{b}$ read

$$I_1(R,t) = 2\frac{\lambda^2(\tau)}{\lambda^2(t)} + \frac{\lambda^4(t)}{\lambda^4(\tau)}, \quad I_2(R,t) = 2\frac{\lambda^2(t)}{\lambda^2(\tau)} + \frac{\lambda^4(\tau)}{\lambda^4(t)}. \tag{2.36}$$

The non-zero components of the Cauchy stress read

$$\begin{aligned} \sigma^{rr}(R,t) &= -p(R,t) + \alpha(R,t)\,\frac{\lambda^2(\tau)}{\lambda^2(t)} - \beta(R,t)\,\frac{\lambda^2(t)}{\lambda^2(\tau(R))}, \\ \sigma^{\theta\theta}(R,t) &= -p(R,t)\,\frac{\lambda^2(t)}{\lambda^2(\tau(R))\,\bar{r}^2(R)} + \alpha(R,t)\,\frac{1}{\bar{r}^2(R)} - \beta(R,t)\,\frac{\lambda^4(t)}{\lambda^4(\tau(R))\,\bar{r}^2(R)}, \\ \sigma^{zz}(R,t) &= -p(R,t) + \alpha(R,t)\,\frac{\lambda^4(t)}{\lambda^4(\tau(R))} - \beta(R,t)\,\frac{\lambda^4(\tau(R))}{\lambda^4(t)}. \end{aligned} \tag{2.37}$$

The equilibrium equation reads $\frac{\partial \sigma^{rr}(R,t)}{\partial R} = 0$. Thus, $\sigma^{rr}(R,t) = \sigma_0(t)$. This implies that

$$-p(R,t) = \sigma_0(t) - \alpha(R,t)\,\frac{\lambda^2(\tau(R))}{\lambda^2(t)} + \beta(R,t)\,\frac{\lambda^2(t)}{\lambda^2(\tau(R))}\,. \tag{2.38}$$

Thus, on the growth surface, one has $-p(s(t),t) = \sigma_0(t) - \alpha(s(t),t) + \beta(s(t),t)$. Hence

$$\boldsymbol{\sigma}(s(t),t) = [-p(s(t),t) + \alpha(s(t),t) - \beta(s(t),t)] \begin{bmatrix} 1 & 0 & 0 \\ 0 & \frac{1}{\bar{r}^2(R)} & 0 \\ 0 & 0 & 1 \end{bmatrix}. \tag{2.39}$$

We know that $\boldsymbol{\sigma}(s(t),t) = \mathbf{0}$,[5] and hence $-p(s(t),t) + \alpha(s(t),t) - \beta(s(t),t) = 0$. This implies that, $\sigma_0(t) = 0$, and thus

$$-p(R,t) = -\alpha(R,t)\,\frac{\lambda^2(\tau(R))}{\lambda^2(t)} + \beta(R,t)\,\frac{\lambda^2(t)}{\lambda^2(\tau(R))}\,. \tag{2.40}$$

Using (2.34) (with $\sigma_0(t) = 0$) and (2.40) one observes that the radial and circumferential (hoop) stresses identically vanish and the only non-zero component of the Cauchy stress has the following distribution

$$\sigma^{zz}(R,t) = \begin{cases} \frac{\lambda^6(t)-1}{\lambda^4(t)}\left[\alpha(R,t)\,\lambda^2(t) + \beta(R,t)\right], & 0 \le R \le R_0\,, \\ \\ \frac{\lambda^6(t)-\lambda^6(\tau(R))}{\lambda^4(\tau(R))\,\lambda^4(t)}\left[\alpha(R,t)\,\lambda^2(t) + \beta(R,t)\,\lambda^2(\tau(R))\right], & R_0 \le R \le s(t)\,. \end{cases} \tag{2.41}$$

Remark 2.4. In anelasticity finite eigenstrains are modeled by the Riemannian metric of the material manifold [Yavari and Goriely, 2013, Yavari, 2021b]. Universal eigenstrains for elastically incompressible isotropic solids were studied by Goodbrake et al. [2020]. They first observed that the known universal deformations of incompressible isotropic solids are invariant under certain Lie subgroups of the special Euclidean group. For each known family of universal deformations, they assumed that the universal eigenstrain distributions, and consequently the corresponding material metrics, are invariant under the same Lie groups. For accreting circular cylindrical bars we assumed the deformation (2.2). Within the initial body ($0 \le R \le R_0$) this is a subset of Family 3 deformations. For the secondary body ($R_0 \le R \le s(t)$), the radial deformation has the form (2.27). We have shown that the following pair of deformations and eigenstrains are universal.[6]

$$\mathbf{G} = \begin{cases} \begin{bmatrix} 1 & 0 & 0 \\ 0 & R^2 & 0 \\ 0 & 0 & 1 \end{bmatrix}, & 0 \le R \le R_0\,, \\ \\ \begin{bmatrix} 1 & 0 & 0 \\ 0 & \bar{r}^2(R) & 0 \\ 0 & 0 & \lambda^4(\tau(R)) \end{bmatrix}, & R_0 \le R \le s(t)\,, \end{cases} \tag{2.42}$$

$$r = \begin{cases} \dfrac{R}{\lambda(t)}\,, & 0 \le R \le R_0\,, \\ \\ \dfrac{1}{\lambda(t)}\left[R_0 + \displaystyle\int_{R_0}^{R} \lambda(\tau(\xi))\,d\xi\right], & R_0 \le R \le s(t) \end{cases}, \quad \theta = \Theta\,, \quad z = \lambda^2(t) Z\,.$$

At the two ends of the bar ($Z = 0, L$), the axial force required to maintain the deformation is calculated as

$$F(t) = 2\pi \int_0^{s(t)} P^{zZ}(R,t) R\,dR\,, \tag{2.43}$$

[5] Note that on the growth surface the entire Cauchy stress is known as the new material added to the boundary in the current configuration is stress-free.

[6] For definition of universal eigenstrains see [Yavari and Goriely, 2016]. See also [Yavari and Pradhan, 2022] for another class of universal deformations and eigenstrains in the case of an accreting circular cylindrical bar under finite torsion.

where P^{zZ} is the zZ-component of the first Piola-Kirchhoff stress, which has the following distribution

$$P^{zZ}(R,t)=\begin{cases}\frac{\lambda^6(t)-1}{\lambda^6(t)}\left[\alpha(R,t)\,\lambda^2(t)+\beta(R,t)\right]\,, & 0\le R\le R_0\,,\\[2ex] \frac{\lambda^6(t)-\lambda^6(\tau(R))}{\lambda^4(\tau(R))\,\lambda^6(t)}\left[\alpha(R,t)\,\lambda^2(t)+\beta(R,t)\,\lambda^2(\tau(R))\right]\,, & R_0\le R\le s(t)\,.\end{cases}\tag{2.44}$$

Example 2.5. For neo-Hookean solids $\alpha(R)=\mu(R)>0$ and $\beta(R)=0$. Let us also assume a uniform shear modulus $\mu(R)=\mu_0$. Thus

$$\sigma^{zz}(R,t)=\begin{cases}\mu_0\,\frac{\lambda^6(t)-1}{\lambda^2(t)}\,, & 0\le R\le R_0\,,\\[2ex] \mu_0\,\frac{\lambda^6(t)-\lambda^6(\tau(R))}{\lambda^4(\tau(R))\,\lambda^2(t)}\,, & R_0\le R\le s(t)\,,\end{cases}\tag{2.45}$$

and

$$P^{zZ}(R,t)=\begin{cases}\mu_0\,\frac{\lambda^6(t)-1}{\lambda^4(t)}\,, & 0\le R\le R_0\,,\\[2ex] \mu_0\,\frac{\lambda^6(t)-\lambda^6(\tau(R))}{\lambda^4(\tau(R))\,\lambda^4(t)}\,, & R_0\le R\le s(t)\,.\end{cases}\tag{2.46}$$

We assume that $R_a=2R_0$, $u_0=1$, and $t_a=1$. In Fig.4, for the displacement-control loading $\lambda(t)=1+\left(\frac{t}{t_a}\right)^3$, we show the distribution of the axial stress for four instances of time during the accretion process.

From (2.43), the axial force is calculated as

$$F(t)=\pi\mu_0R_0^2\,\frac{\lambda^6(t)-1}{\lambda^4(t)}+2\pi\mu_0\int_{R_0}^{R_0+u_0t}R\left[\frac{\lambda^2(t)}{\lambda^4(\tau(R))}-\frac{\lambda^2(\tau(R))}{\lambda^4(t)}\right]dR\,.\tag{2.47}$$

If $F(t)$ is given, the nonlinear integral equation (2.47) needs to be solved numerically to find $\lambda(t)$. In order to numerically solve this integral equation using Mathematica we first transform it to a system of first-order ODEs. Let us define

$$h_1(t)=\int_{R_0}^{s(t)}R\,\lambda^{-4}(\tau(R))\,dR\,,\quad h_2(t)=\int_{R_0}^{s(t)}R\,\lambda^2(\tau(R))\,dR\,.\tag{2.48}$$

Note that $h_1(0)=h_2(0)=0$. Now the nonlinear integral equation (2.47) can be rewritten as

$$\begin{cases}h_1'(t)=u_0\,s(t)\,\lambda^{-4}(t)\,,\\ h_2'(t)=u_0\,s(t)\,\lambda^2(t)\,,\\ \lambda^2(t)-\lambda^{-4}(t)+\dfrac{2}{R_0^2}\left[h_1(t)\,\lambda^2(t)-h_2(t)\,\lambda^{-4}(t)\right]=f(t)\,,\\ h_1(0)=h_2(0)=0\,,\ \lambda(0)=1\,.\end{cases}\tag{2.49}$$

Example 2.6. We consider the following applied forces:

$$\begin{aligned}F_1^{\pm}(t)&=\pm\mu_0\,\pi R_0^2\,\sin\Big(\frac{2\pi t}{t_a}\Big)\,,\\ F_2^{\pm}(t)&=\pm\mu_0\,\pi R_0^2\,\sin\Big(\frac{4\pi t}{t_a}\Big)\,,\\ F_3^{\pm}(t)&=\pm\mu_0\,\pi R_0^2\,\sin^2\Big(\frac{2\pi t}{t_a}\Big)\,,\\ F_4^{\pm}(t)&=\pm\mu_0\,\pi R_0^2\,\sin^2\Big(\frac{4\pi t}{t_a}\Big)\,.\end{aligned}\tag{2.50}$$

We assume that $R_a=2R_0$, $u_0=1$, and $t_a=1$. The corresponding $\lambda^2(t)$ are shown in Fig.5.

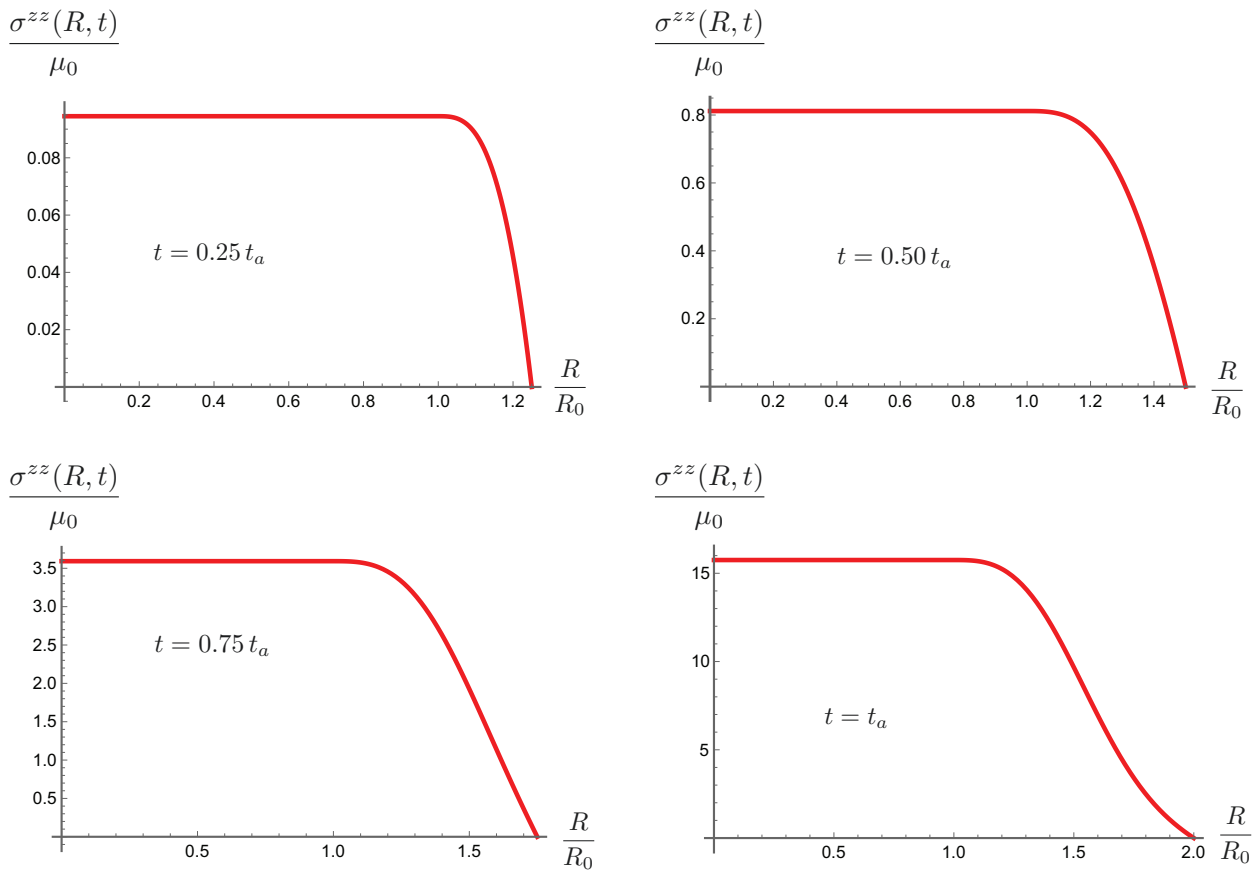

Figure 4: *Axial stress distribution during the accretion process at four different instances of time for the displacement-control loading* $\lambda(t) = 1 + \left(\frac{t}{t_a}\right)^3$.

2.1 Residual stresses

We assume that the accretion process starts at time $t = 0$ and ends at time $t = t_a$. For any $t > t_a$, if the body is unloaded, i.e., $\lambda(t) = 1$ (or equivalently $F(t) = 0$), the accreted bar may be residually stressed. Residual stresses depend on the growth velocity and the history of deformation in the interval $[0, t_a]$. The material metric of the accreted bar has the following representation

$$\begin{aligned} 0 \le R \le R_0 : \quad \mathbf{G} &= \begin{bmatrix} 1 & 0 & 0 \\ 0 & R^2 & 0 \\ 0 & 0 & 1 \end{bmatrix}, \\ R_0 \le R \le R_a : \quad \mathbf{G} &= \begin{bmatrix} 1 & 0 & 0 \\ 0 & \bar{r}^2(R) & 0 \\ 0 & 0 & \lambda^4(\tau(R)) \end{bmatrix}, \end{aligned} \tag{2.51}$$

where $R_a = s(t_a)$. Let us denote the mapping from the material manifold to the residually-stressed configuration by $\tilde{\varphi} : \mathcal{B} \to \mathcal{S}$, where in cylindrical coordinates: $\tilde{\varphi}(R, \Theta, Z) = (\tilde{r}, \tilde{\theta}, \tilde{z}) = (\tilde{r}(R), \Theta, \tilde{\lambda}^2 Z)$, and $\tilde{\lambda}^2$ is the residual stretch (see Figs. 1 and 2). Incompressibility implies that

$$\begin{aligned} \tilde{r}(R) &= \frac{R}{\tilde{\lambda}}, && 0 \le R \le R_0, \\ \tilde{r}^2(R) &= \frac{R_0^2}{\tilde{\lambda}^2} + \frac{2}{\tilde{\lambda}^2} \int_{R_0}^{R} \bar{r}(\xi)\, \lambda^2(\tau(\xi))\, d\xi, && R_0 \le R \le R_a. \end{aligned} \tag{2.52}$$

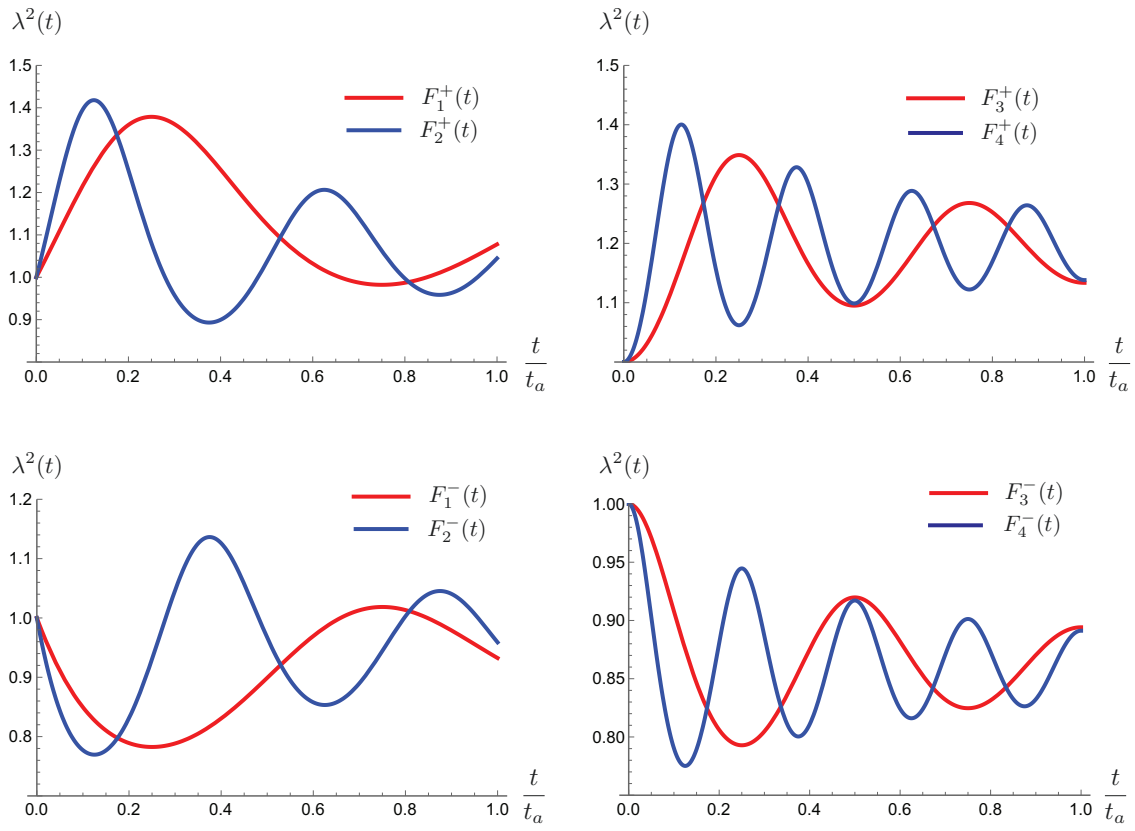

Figure 5: $\lambda^2(t)$ *distribution for eight different loadings during accretion.*

For the deformation mapping $\tilde{\varphi}$ the principal invariants read

$$\begin{aligned} I_1(R) &= \frac{2+\tilde{\lambda}^6}{\tilde{\lambda}^2}\,, \quad I_2(R) = \frac{1+2\tilde{\lambda}^6}{\tilde{\lambda}^4}\,, && R_1 \le R \le R_0, \\ I_1(R) &= 2\frac{\lambda^2(\tau)}{\lambda^2(t)} + \frac{\lambda^4(t)}{\lambda^4(\tau)}\,, \quad I_2(R) = 2\frac{\tilde{\lambda}^2}{\lambda^2(\tau(R))} + \frac{\lambda^4(\tau(R))}{\tilde{\lambda}^4}\,, && R_0 \le R \le R_a. \end{aligned} \tag{2.53}$$

The radial and circumferential stress components are identically zero everywhere and hence the boundary condition $\tilde{\sigma}^{rr}(R_a) = 0$ is trivially satisfied. The axial stress component has the following distribution

$$\tilde{\sigma}^{zz}(R,t) = \begin{cases} \frac{\tilde{\lambda}^6-1}{\tilde{\lambda}^4}\left[\alpha(R)\,\tilde{\lambda}^2 + \beta(R)\right]\,, & 0 \le R \le R_0\,, \\ \frac{\tilde{\lambda}^6-\lambda^6(\tau(R))}{\lambda^4(\tau(R))\,\tilde{\lambda}^4}\left[\alpha(R)\,\tilde{\lambda}^2 + \beta(R)\,\lambda^2(\tau(R))\right]\,, & R_0 \le R \le R_a\,. \end{cases} \tag{2.54}$$

Similarly, the axial component of the first Piola-Kirchhoff stress has the distribution

$$\tilde{P}^{zZ}(R,t) = \begin{cases} \frac{\tilde{\lambda}^6-1}{\tilde{\lambda}^6}\left[\alpha(R)\,\tilde{\lambda}^2 + \beta(R)\right]\,, & 0 \le R \le R_0\,, \\ \frac{\tilde{\lambda}^6-\lambda^6(\tau(R))}{\lambda^4(\tau(R))\,\tilde{\lambda}^6}\left[\alpha(R)\,\tilde{\lambda}^2 + \beta(R)\,\lambda^2(\tau(R))\right]\,, & R_0 \le R \le s(t)\,. \end{cases} \tag{2.55}$$

The unknown residual stretch is calculated using the condition $F = 0$.

	$m=\frac{1}{3}$	$m=\frac{1}{2}$	$m=1$	$m=2$	$m=3$
$\lambda(t)=1+\left(\frac{t}{t_a}\right)^m$	1.20089	1.19249	1.17085	1.13907	1.11709
$\lambda(t)=1-\frac{1}{2}\left(\frac{t}{t_a}\right)^m$	0.593063	0.623043	0.686102	0.758822	0.802297

Table 1: *Residual stretch for different displacement-control loadings. In the first row stretch varies from* 1.0 *to* 2.0 *in the time interval* $[0,t_a]$. *In the second row it varies from* 1.0 *to* 0.5 *in the time interval* $[0,t_a]$.

Example 2.7. For a homogeneous neo-Hookean bar $\alpha(R)=\mu_0>0$ and $\beta(R)=0$. Thus

$$\tilde{\sigma}^{zz}(R,t)=\begin{cases}\mu_0\,\frac{\tilde{\lambda}^6-1}{\tilde{\lambda}^2}\,, & 0\le R\le R_0\,,\\[2ex] \mu_0\left[\frac{\tilde{\lambda}^4}{\lambda^4(\tau(R))}-\frac{\lambda^2(\tau(R))}{\tilde{\lambda}^2}\right], & R_0\le R\le R_a\,,\end{cases}\tag{2.56}$$

and $\tilde{P}^{zZ}(R,t)=\frac{\tilde{\sigma}^{zz}(R,t)}{\tilde{\lambda}^2}$. The condition $F=0$ is simplified to read

$$\tilde{\lambda}^6+\frac{2}{R_0^2\,\tilde{\lambda}^4}\int_{R_0}^{R_a}R\left[\frac{\tilde{\lambda}^2}{\lambda^4(\tau(R))}-\frac{\lambda^2(\tau(R))}{\tilde{\lambda}^4}\right]dR=1\,.\tag{2.57}$$

Let us assume that $R_a=2R_0$. Thus $t_a u_0=R_0$. We also assume that $u_0=1.0$, and consider two displacement-control loadings during the accretion process: i) $\lambda(t)=1+\left(\frac{t}{t_a}\right)^m$, $m>0$. In this loading the stretch monotonically increases from 1.0 to 2.0 in the interval $[0,t_a]$. ii) $\lambda(t)=1-\frac{1}{2}\left(\frac{t}{t_a}\right)^m$, $m>0$. In this loading the stretch monotonically decreases from 1.0 to 0.5 in the interval $[0,t_a]$. In Table 1 we show the residual stretches for five different values of m for the two loadings. In Fig.6, the residual axial stress distribution for four different displacement-control loadings during the accretion process are shown.

2.2 Linearized accretion mechanics

Linearized kinematics. Next we linearize the governing equations of the nonlinear accretion theory and find those of the linearized accretion mechanics. We assume that linearization is with respect to an undeformed stress-free configuration of the bar. More precisely, let us consider a reference motion $\mathring{\varphi}_t$, and a one-parameter family of motions $\varphi_{t,\epsilon}$ such that $\varphi_{t,0}=\mathring{\varphi}_t$ [Marsden and Hughes, 1983, Yavari and Ozakin, 2008, Sozio and Yavari, 2017]. For the finite extension of a bar we consider the one-parameter family of motions $\varphi_\epsilon(R,\Theta,Z,t)=(r_\epsilon(R,t),\Theta,\lambda_\epsilon^2(t)Z)$. We linearize the governing equations with respect to the reference motion $\mathring{\varphi}_t(R,\Theta,Z,t)=(R,\Theta,Z)$, which corresponds to the motion of a cylindrical bar that is under no external forces while stress-free cylindrical layers are added to its boundary cylinder in the time interval $[0,t_a]$. The variation field is defined as

$$\delta\varphi_t(R,\Theta,Z)=\frac{d}{d\epsilon}\Big|_{\epsilon=0}\varphi_\epsilon(R,\Theta,Z,t)=(\delta r(R,t),0,2\delta\lambda(t)\,Z)\,.\tag{2.58}$$

From, $\delta r(R,t)=\frac{d}{d\epsilon}\Big|_{\epsilon=0}r_\epsilon(R,t)$, one concludes that $\delta\bar{r}(R)=\delta r\Big(R,\frac{R-R_0}{u_0}\Big)$. The displacement field is defined as

$$\mathbf{U}(R,\Theta,Z,t)=\delta\varphi_t(R,\Theta,Z)-\delta\varphi_{\tau(R)}(R,\Theta,Z)\,.\tag{2.59}$$

Assuming that $\lambda(0)=1$, for the initial body $(0\le R\le R_0)$, $\varphi_\epsilon(R,\Theta,Z,0)=(r_\epsilon(R,0),\Theta,Z)=(R,\Theta,Z)$, and hence $\delta\varphi_0(R,\Theta,Z)=(0,0,0)$. Thus, for $0\le R\le R_0$, $\mathbf{U}(R,\Theta,Z,t)=\delta\varphi_t(R,\Theta,Z)$. However, for the new material points $(R_0\le R\le s(t)=R_0+u_0t)$ the displacement field is defined with respect to their positions at the time of attachment.

For $0\le R\le R_0$, the incompressibility condition for the perturbed motions along with $r_\epsilon(0,t)=0$, implies that

$$r_\epsilon(R,t)=\frac{R}{\lambda_\epsilon(t)}\,,\qquad 0\le R\le R_0\,.\tag{2.60}$$

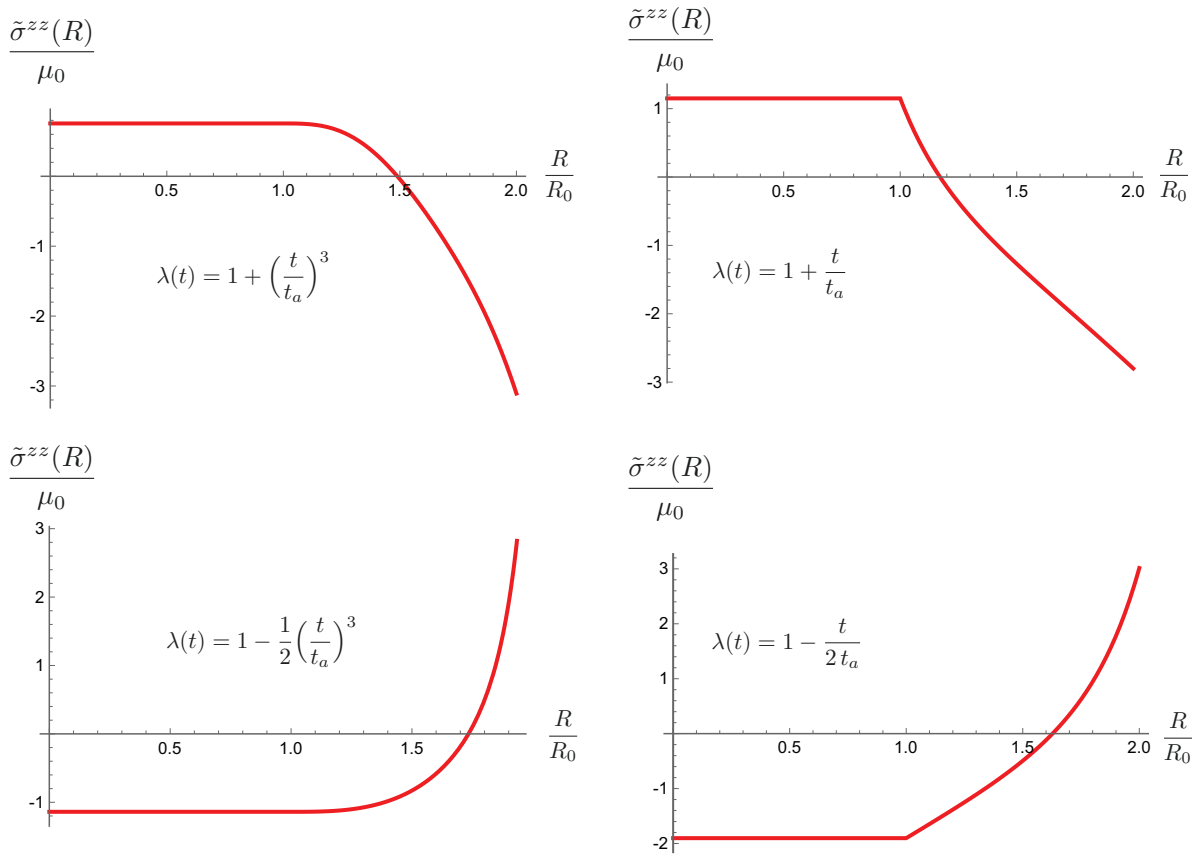

Figure 6: *Axial residual stress distribution for different displacement-control loadings during the accretion process.*

Taking derivative with respect to ϵ on both sides, evaluating at $\epsilon = 0$, and noting that $\lambda_{\epsilon=0}(t) = 1$, one obtains

$$\delta r(R,t) = -R\,\delta\lambda(t)\,. \tag{2.61}$$

Knowing that $\lambda_\epsilon(0) = 1$, $\delta\lambda(0) = 0$, and hence $\delta r(R,0) = 0$.

For $R_0 \le R \le s(t)$:

$$r_\epsilon(R,t) = \frac{1}{\lambda_\epsilon(t)}\left[R_0 + \int_{R_0}^{R} \lambda_\epsilon(\tau(\xi))\,d\xi\right]\,. \tag{2.62}$$

Thus

$$\delta r(R,t) = -R\,\delta\lambda(t) + \int_{R_0}^{R} \delta\lambda(\tau(\xi))\,d\xi\,. \tag{2.63}$$

Linearized stresses. The only non-zero component of the Cauchy stress for the perturbed motion of a homogeneous bar made of a neo-Hookean solid is

$$\sigma_\epsilon^{zz}(R,t) = \begin{cases} \mu_0\,\frac{\lambda_\epsilon^6(t)-1}{\lambda_\epsilon^2(t)}\,, & 0 \le R \le R_0\,, \\ \mu_0\left[\frac{\lambda_\epsilon^4(t)}{\lambda_\epsilon^4(\tau(R))} - \frac{\lambda_\epsilon^2(\tau(R))}{\lambda_\epsilon^2(t)}\right]\,, & R_0 \le R \le s(t)\,. \end{cases} \tag{2.64}$$

Therefore

$$\delta\sigma^{zz}(R,t)=\begin{cases}6\mu_0\,\delta\lambda(t)\,, & 0\le R\le R_0\,,\\[2mm] 6\mu_0\left[\delta\lambda(t)-\delta\lambda(\tau(R))\right]\,, & R_0\le R\le s(t)\,.\end{cases}\tag{2.65}$$

For the perturbed motion the axial force is calculated as

$$F_\epsilon(t)=\pi\mu_0R_0^2\,\frac{\lambda_\epsilon^6(t)-1}{\lambda_\epsilon^4(t)}+2\pi\mu_0\int_{R_0}^{s(t)}R\left[\frac{\lambda_\epsilon^2(t)}{\lambda_\epsilon^4(\tau(R))}-\frac{\lambda_\epsilon^2(\tau(R))}{\lambda_\epsilon^4(t)}\right]dR\,.\tag{2.66}$$

Thus

$$\begin{aligned}\delta F(t)&=6\pi\mu_0R_0^2\,\delta\lambda(t)+12\pi\mu_0\int_{R_0}^{s(t)}R\left[\delta\lambda(t)-\delta\lambda(\tau(R))\right]dR\\&=6\pi\mu_0s^2(t)\,\delta\lambda(t)-12\pi\mu_0\int_{R_0}^{s(t)}R\delta\lambda(\tau(R))\,dR\,.\end{aligned}\tag{2.67}$$

Taking time derivative of both sides, one obtains

$$\frac{\dot{\overline{\delta F(t)}}}{6\pi\mu_0}=2s(t)\dot{s}(t)\,\delta\lambda(t)+s^2(t)\,\dot{\overline{\delta\lambda(t)}}-2\dot{s}(t)s(t)\,\delta\lambda(\tau(s(t)))=s^2(t)\,\dot{\overline{\delta\lambda(t)}}\,.\tag{2.68}$$

This implies that

$$\dot{\overline{\delta\lambda(t)}}=\frac{\dot{\overline{\delta F(t)}}}{6\pi\mu_0\,s^2(t)}\,.\tag{2.69}$$

Therefore

$$\delta\lambda(t)=\frac{1}{6\pi\mu_0}\int_0^t\frac{\dot{\overline{\delta F(\eta)}}}{s^2(\eta)}\,d\eta\,.\tag{2.70}$$

In particular, one obtains

$$\delta\lambda(\tau(R))=\frac{1}{6\pi\mu_0}\int_0^{\tau(R)}\frac{\dot{\overline{\delta F(\eta)}}}{s^2(\eta)}\,d\eta\,.\tag{2.71}$$

Example 2.8. Let us consider the applied force $F(t)=k\mu_0\pi R_0^2\sin^2\!\left(\frac{2\pi t}{t_a}\right)$ in both the nonlinear and linearized solutions. We assume that $R_a=2R_0$, $u_0=1$, and $t_a=1$. In Fig.7 we compare the nonlinear axial stretch $\lambda^2(t)$ and its linearization $1+2\delta\lambda(t)$ for three values of $k=0.25,0.5$, and 1.0. It is observed that for small applied loads (here $k=0.25$) the two solutions agree. However, for large loads the linearized theory underestimates the axial stretch.

Linearized residual stretch and residual stresses. The zero applied force for the perturbed motion using (2.66) is written as

$$R_0^2\,\frac{\tilde\lambda_\epsilon^6-1}{\tilde\lambda_\epsilon^4}+2\int_{R_0}^{R_a}R\left[\frac{\tilde\lambda_\epsilon^2}{\lambda_\epsilon^4(\tau(R))}-\frac{\lambda_\epsilon^2(\tau(R))}{\tilde\lambda_\epsilon^4}\right]dR=0\,.\tag{2.72}$$

Taking derivative with respect to ϵ and evaluating at $\epsilon=0$, one obtains

$$\delta\tilde\lambda=\frac{2}{R_a^2}\int_{R_0}^{R_a}R\delta\lambda(\tau(R))\,dR=\frac{1}{3\pi\mu_0\,R_a^2}\int_{R_0}^{R_a}R\int_0^{\tau(R)}\frac{\dot{\overline{\delta F(\eta)}}}{s^2(\eta)}\,d\eta\,dR\,.\tag{2.73}$$

The linearized residual axial stress has the following distribution

$$\delta\tilde\sigma^{zz}(R)=\begin{cases}6\mu_0\,\delta\tilde\lambda\,, & 0\le R\le R_0\,,\\[2mm] 6\mu_0\left[\delta\tilde\lambda-\delta\lambda(\tau(R))\right]\,, & R_0\le R\le R_a\,.\end{cases}\tag{2.74}$$

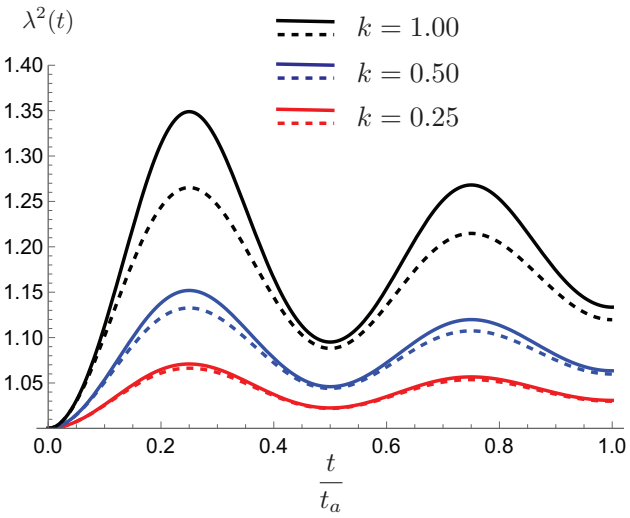

Figure 7: *Comparison of the nonlinear and linearized axial stretches for the applied load* $F(t) = k\,\mu_0 \pi R_0^2 \sin^2\left(\frac{2\pi t}{t_a}\right)$ *for three different values of* k*. The solid and dashed curves are the nonlinear and linear solutions, respectively.*

3 Conclusions

In this paper we formulated the initial-boundary-value problem of accretion of a solid circular cylinder under finite time-dependent extensions. More specifically, while the bar is under a time-dependent axial stretch stress-free cylindrical layers are continuously added to it. Starting from a stress-free initial bar, the accreted bar after the removal of external forces is not stress-free, in general. The state of residual stresses depends on the history of the deformation during the accretion process. We modeled the natural configuration of the accreting cylinder by a Riemannian manifold whose metric explicitly depends on the deformation history during the accretion process. Assuming that the bar is made of an arbitrary incompressible isotropic solid we showed that the radial motion is completely determined by the axial stretch function. Consequently, residual stresses are determined as soon as one computes the residual stretch. We considered both displacement-control and force-control loadings during accretion. In the case of force-control loading the time-dependent axial stretch was calculated numerically in a few examples. We also numerically showed that residual stretch explicitly depends on the history of deformation during the accretion process. Finally, we derived analytic expressions for stresses, residual stretch, and residual stresses in the accreting bar in the setting of linear accretion mechanics. We compared the nonlinear and linear solutions for stretch during accretion under a few force-control loading examples. As expected, for small applied forces the linearized solution is a good approximation. For large applied forces, however, the linearized solution considerably underestimates the axial stretch. A thermoelastic analysis of accretion under finite time-dependent extensions, and dynamic analysis of accreted bars under pulse or impact loads will be future extensions of this work.

Acknowledgement

This research was partially supported by the Swiss National Science Foundation Grant No. IZSE0-187171/1, NSF – Grant No. CMMI 1939901, and ARO Grant No. W911NF-18-1-0003.

References

R. Abi-Akl and T. Cohen. Surface growth on a deformable spherical substrate. *Mechanics Research Communications*, 103:103457, 2020.

R. Abi-Akl, R. Abeyaratne, and T. Cohen. Kinetics of surface growth with coupled diffusion and the emergence of a universal growth path. *Proceedings of the Royal Society A*, 475(2221):20180465, 2019.

S. Afazov, W. A. Denmark, B. L. Toralles, A. Holloway, and A. Yaghi. Distortion prediction and compensation in selective laser melting. *Additive Manufacturing*, 17:15–22, 2017.

N. K. Arutyunyan, V. Naumov, and Y. N. Radaev. A mathematical model of a dynamically accreted deformable body. part 1: Kinematics and measure of deformation of the growing body. *Izv. Akad. Nauk SSSR. Mekh. Tverd. Tela*, (6):85–96, 1990.

G. L. Bergel and P. Papadopoulos. A finite element method for modeling surface growth and resorption of deformable solids. *Computational Mechanics*, 68(4):759–774, 2021.

C. B. Brown and L. E. Goodman. Gravitational stresses in accreted bodies. *Proceedings of the Royal Society of London A*, 276(1367):571–576, 1963.

K. Carpenter and A. Tabei. On residual stress development, prevention, and compensation in metal additive manufacturing. *Materials*, 13(2):255, 2020.

P. A. Colegrove, J. Donoghue, F. Martina, J. Gu, P. Prangnell, and J. Hönnige. Application of bulk deformation methods for microstructural and material property improvement and residual stress and distortion control in additively manufactured components. *Scripta Materialia*, 135:111–118, 2017.

T. C. Doyle and J. L. Ericksen. Nonlinear elasticity. *Advances in Applied Mechanics*, 4:53–115, 1956.

A. D. Drozdov. Continuous accretion of a composite cylinder. *Acta Mechanica*, 128(1), 1998a.

A. D. Drozdov. *Viscoelastic Structures: Mechanics of Growth and Aging*. Academic Press, 1998b.

C. Eckart. The thermodynamics of irreversible processes. 4. the theory of elasticity and anelasticity. *Physical Review*, 73(4):373–382, 1948.

M. Epstein. Kinetics of boundary growth. *Mechanics Research Communications*, 37(5):453–457, 2010.

J. L. Ericksen. Deformations possible in every isotropic, incompressible, perfectly elastic body. *Zeitschrift für Angewandte Mathematik und Physik*, 5(6):466–489, 1954.

C. Goodbrake, A. Yavari, and A. Goriely. The anelastic Ericksen problem: Universal deformations and universal eigenstrains in incompressible nonlinear anelasticity. *Journal of Elasticity*, 142(2):291–381, 2020.

J. Kadish, J. Barber, and P. Washabaugh. Stresses in rotating spheres grown by accretion. *International Journal of Solids and Structures*, 42(20):5322–5334, 2005.

N. Kalentics, E. Boillat, P. Peyre, C. Gorny, C. Kenel, C. Leinenbach, J. Jhabvala, and R. E. Logé. 3d laser shock peening–a new method for the 3d control of residual stresses in selective laser melting. *Materials & Design*, 130:350–356, 2017.

S. Lychev and A. Manzhirov. The mathematical theory of growing bodies. Finite deformations. *Journal of Applied Mathematics and Mechanics*, 77(4):421–432, 2013.

S. Lychev, K. Koifman, and N. Djuzhev. Incompatible deformations in additively fabricated solids: Discrete and continuous approaches. *Symmetry*, 13(12):2331, 2021.

S. A. Lychev. Geometric aspects of the theory of incompatible deformations in growing solids. In *Mechanics for Materials and Technologies*, pages 327–347. Springer, 2017.

A. Manzhirov. The general non-inertial initial-boundaryvalue problem for a viscoelastic ageing solid with piecewise-continuous accretion. *Journal of Applied Mathematics and Mechanics*, 59(5):805–816, 1995.

A. V. Manzhirov. Mechanics of growing solids: New track in mechanical engineering. In *ASME 2014 International Mechanical Engineering Congress and Exposition*, pages V009T12A039–V009T12A039. American Society of Mechanical Engineers, 2014.

J. Marsden and T. Hughes. *Mathematical Foundations of Elasticity*. Dover, 1983.

V. Metlov. On the accretion of inhomogeneous viscoelastic bodies under finite deformations. *Journal of Applied Mathematics and Mechanics*, 49(4):490–498, 1985.

V. E. Naumov. Mechanics of growing deformable solids: a review. *Journal of Engineering Mechanics*, 120 (2):207–220, 1994.

A. Nazarov, V. Vivier, F. Vucko, and D. Thierry. Effect of tensile stress on the passivity breakdown and repassivation of aisi 304 stainless steel: A scanning Kelvin probe and scanning electrochemical microscopy study. *Journal of The Electrochemical Society*, 166(11):C3207, 2019.

R. W. Ogden. *Non-Linear Elastic Deformations*. Courier Corporation, 1997.

J. J. Ong and O. M. O'Reilly. On the equations of motion for rigid bodies with surface growth. *International Journal of Engineering Science*, 42(19):2159–2174, 2004.

H. Poincaré. *Science and Hypothesis*. Science Press, 1905.

J. Simo and J. Marsden. Stress tensors, Riemannian metrics and the alternative descriptions in elasticity. In *Trends and Applications of Pure Mathematics to Mechanics*, pages 369–383. Springer, 1984.

R. Southwell. *Introduction to the Theory of Elasticity for Engineers and Physicists*. Oxford University Press, 1941.

F. Sozio and A. Yavari. Nonlinear mechanics of surface growth for cylindrical and spherical elastic bodies. *Journal of the Mechanics and Physics of Solids*, 98:12–48, 2017.

F. Sozio and A. Yavari. Nonlinear mechanics of accretion. *Journal of Nonlinear Science*, 29(4):1813–1863, 2019.

F. Sozio, M. Faghih Shojaei, S. Sadik, and A. Yavari. Nonlinear mechanics of thermoelastic accretion. *Zeitschrift für angewandte Mathematik und Physik*, 71(3):1–24, 2020.

R. Tangestani, G. H. Farrahi, M. Shishegar, B. P. Aghchehkandi, S. Ganguly, and A. Mehmanparast. Effects of vertical and pinch rolling on residual stress distributions in wire and arc additively manufactured components. *Journal of Materials Engineering and Performance*, 29(4):2073–2084, 2020.

G. Tomassetti, T. Cohen, and R. Abeyaratne. Steady accretion of an elastic body on a hard spherical surface and the notion of a four-dimensional reference space. *Journal of the Mechanics and Physics of Solids*, 96: 333–352, 2016.

L. Truskinovsky and G. Zurlo. Nonlinear elasticity of incompatible surface growth. *Physical Review E*, 99 (5):053001, 2019.

A. Yavari. Universal deformations in inhomogeneous isotropic nonlinear elastic solids. *Proceedings of the Royal Society A*, 477(2253):20210547, 2021a.

A. Yavari. On eshelby's inclusion problem in nonlinear anisotropic elasticity. *Journal of Micromechanics and Molecular Physics*, 6(01):2150002, 2021b.

A. Yavari and A. Goriely. Nonlinear elastic inclusions in isotropic solids. *Proceedings of the Royal Society A*, 469(2160):20130415, 2013.

A. Yavari and A. Goriely. The anelastic ericksen problem: Universal eigenstrains and deformations in compressible isotropic elastic solids. *Proceedings of the Royal Society A*, 472(2196):20160690, 2016.

A. Yavari and A. Goriely. Universal deformations in anisotropic nonlinear elastic solids. *Journal of the Mechanics and Physics of Solids*, 156:104598, 2021.

A. Yavari and A. Goriely. The universal program of nonlinear hyperelasticity. *Journal of Elasticity*, 2022.

A. Yavari and A. Ozakin. Covariance in linearized elasticity. *Zeitschrift für Angewandte Mathematik und Physik*, 59(6):1081–1110, 2008.

A. Yavari and S. P. Pradhan. Accretion mechanics of nonlinear elastic circular cylindrical bars under finite torsion. *Journal of Elasticity*, pages 1–32, 2022.

J. Zhu and W. Yuan. Effect of pre-stretching on residual stresses and microstructures of inconel 718 superalloy. *Metals*, 11(4):614, 2021.

G. Zurlo and L. Truskinovsky. Printing non-Euclidean solids. *Physical Review Letters*, 119(4):048001, 2017.

G. Zurlo and L. Truskinovsky. Inelastic surface growth. *Mechanics Research Communications*, 93:174–179, 2018.